
Article:
Tsevas, K., Smith, J.A. orcid.org/0000-0001-6889-4408, Kumar, V. et al. (7 more authors) (2021) Controlling PbI2 stoichiometry during synthesis to improve the performance of perovskite photovoltaics. Chemistry of Materials, 33 (2). pp. 554-566. ISSN 0897-4756

https://doi.org/10.1021/acs.chemmater.0c03517

Supporting Information

Controlling PbI_2 stoichiometry during synthesis to improve the performance of perovskite photovoltaics

Konstantinos Tsevas[a], *Joel A. Smith*[b], *Vikas Kumar*[c], *Cornelia Rodenburg*[c], Mihalis Fakis[d], *Abd. Rashid bin Mohd Yusoff,*[e], Maria Vasilopoulou,[f], *David G. Lidzey*[b], *Mohammad K. Nazeeruddin*[g] *and Alan D. F. Dunbar*[a,*]

[a] Department of Chemical and Biological Engineering, University of Sheffield, Mappin Street, Sheffield S1 3JD, U.K.

[b] Department of Physics & Astronomy, University of Sheffield, Hicks Building, Hounsfield Road, Sheffield, S3 7RH, U.K.

[c] Department of Materials Science and Engineering, University of Sheffield, Mappin Street, Sheffield S1 3JD, U.K.

[d] Department of Physics, University of Patras, 26504, Rio Patras, Greece

[e]Department of Physics, Swansea University, Vivian Tower, Singleton Park, SA2 8PP Swansea, U.K.

[f]Institute of Nanoscience and Nanotechnology, National Centre for Scientific Research Demokritos, 15341 Agia Paraskevi, Attica, Greece

[g]Group for Molecular Engineering of Functional Materials, Institute of Chemical Sciences and Engineering, École Polytechnique Fédérale de Lausanne (EPFL), Rue de l'Industrie 17, CH-1951 Sion, Switzerland.

Corresponding author: a.dunbar@sheffield.ac.uk

Section 1: Theory of polytypism

One of the most prevalent theories presented by Frank, ascribes the formation of polytypes to crystallographic mismatches during the spiral growth of screw dislocations.[1] In this theory, PbI_2 platelet shaped structures are initially formed by surface nucleation and then grow layer-by-layer under saturated in iodide. These platelets might contain crystallographic defects such as twins, stacking faults or result in syntactic coalescence of more than one polytype, due to thermodynamic fluctuations during the growth process, resulting in sub- or over-stoichiometric PbI_2. Consequently, Pandey and Krishna proposed a complicated faulted basic matrix model to provide a theoretical description of polytypism, governed by three major parameters: i) the energy of the fault near the surface of the matrix, during the formation of the screw dislocation, ii) the energy of the screw dislocation and iii) the stacking fault energy of the formatted polytype.[2-4] The letter "H", in the polytype description indicates the hexagonal cells, as opposed to rhombohedral ("R") and cubic ("C") cells, based on Ramsdell notation.[5]

Table S1. Scanning electron microscopy-energy dispersive spectroscopy (SEM-EDS) data indicating atomic percentage composition of lead iodide, synthesised by hydrothermal or mechanochemical methods.

	Hydrothermal				**Mechanochemical**	
Points	1	2	3	4	All image	
Carbon	12.37%	15.68%	11.15%	12.61%	15.80%	12.26%
Oxygen	8.93%	7.42%	14.52%	None detected	None detected	None detected
Iodide	38.68%	41.32%	36.00%	56.87%	56.26%	58.26%
Lead	40.02%	35.58%	38.07%	30.52%	27.94%	29.48%

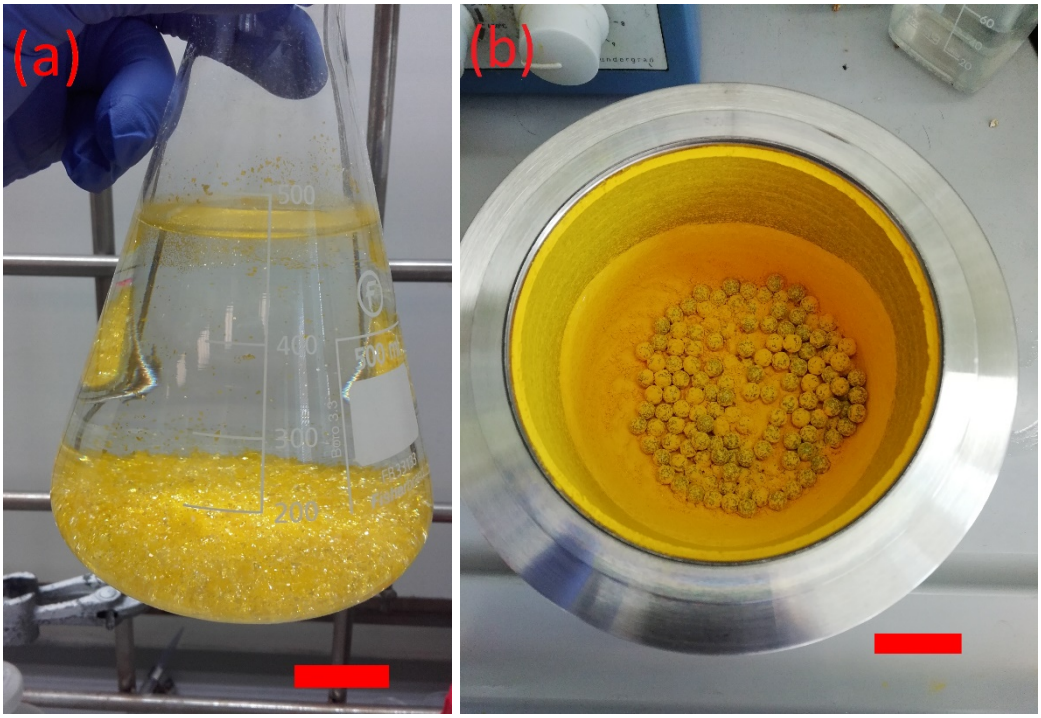

Figure S1. Images of (a) hydrothermal and (b) mechanochemical synthesised lead iodide powders, scale bars represent 2 cm.

Table S2. XRD diffracted angle (2-theta), Miller indices and polytypic phases present in respect to diffraction angle of 2H – 4H – 14H – 20H polytypic phases of lead iodide. (Source: International Centre for Diffraction Database).

2-theta (degrees)	2H polytypic phase	Intensity	4H polytypic phase	Intensity	14H polytypic phase	Intensity	20H polytypic phase	Intensity	Polytypic phases present in respect to diffraction angle
	Miller indices		Miller indices		Miller indices		Miller indices		
12.74	(0 0 1)	314	(0 0 2)	777	(0 0 7)	519	(0 0 10)	577	2H – 4H – 14H – 20H
22.60			(1 0 0)	73	(1 0 0)	32*10^6	(0 1 2)	16	14H
25.56	(0 1 1)	1000	(0 0 4)	21	(0 0 14)	22	(0 0 20)	26	2H
25.98			(1 0 2)	798	(1 0 7)	1000	(0 1 10)	1000	4H – 14H – 20H
34.32			(0 1 4)	176	(1 0 14)	459	(0 1 20)	420	4H – 14H – 20H
38.70	(0 0 3)	36	(1 1 0)	10^9	(0 1 17)	42*10^6	(0 0 30)	36	2H – 4H – 14H – 20H
39.58			(1 1 1)	13	(1 1 0)	471	(1 1 0)	524*10^6	14H – 20H
41.70			(1 1 2)	228	(1 0 19)	19	(1 1 10)	169*10^6	20H
45.27			(2 0 0)	10	(2 0 0)	6*10^6	(2 0 0)	7*10^6	14H – 20H
47.92					(2 0 7)	161	(0 2 11)	21	14H – 20H

Section 2: XPS analysis of PbI_2

Inhomogeneity can affect the relative intensity of the emission peaks in XPS, as a consequence of the signal attenuation from the scattered electrons that varies as a function of the kinetic energy of the emitted electrons. Also, X-rays promote the photolysis of the PbI_2 during the XPS analytical conditions, as presented by Watson *et al.*[6] The XPS spectra acquisition sequence used (survey scan followed by high-resolution scan or single high-resolution scan) can introduce variations between the lead to iodide ratio, due to the interaction of photons with iodide and result in an enhanced signal corresponding to metallic lead. This effect was confirmed by comparing a survey followed by high-resolution scan and a single high-resolution scan

without any survey collected from two identical TCI samples, as shown in Figures S2a and S2b, respectively. The lead to iodide ratio in the TCI sample was 1:2.3 (± 0.1), when a survey followed by a high-resolution scan as acquisition mode of signal was applied, while a ratio of 1:2.4 (± 0.1), when a single high-resolution scan as an acquisition mode of signal was applied.

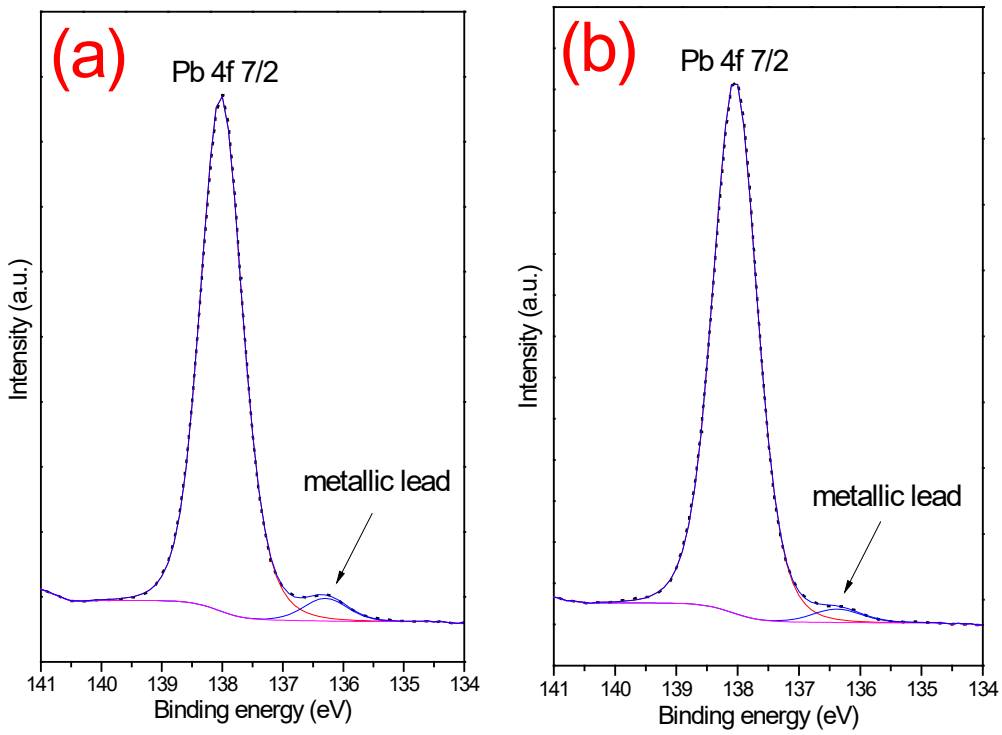

Figure S2. XPS single high-resolution spectra of Pb 4f 7/2 core level and metallic lead for the TCI lead iodide from different scanning modes. (a) survey followed by high-resolution scans and (b) single high-resolution scan.

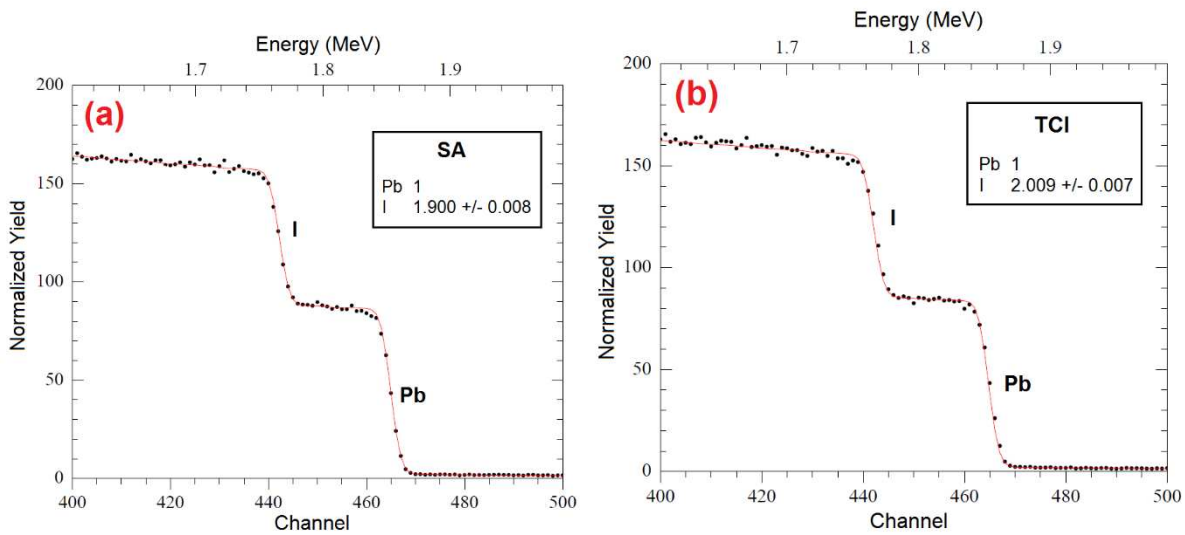

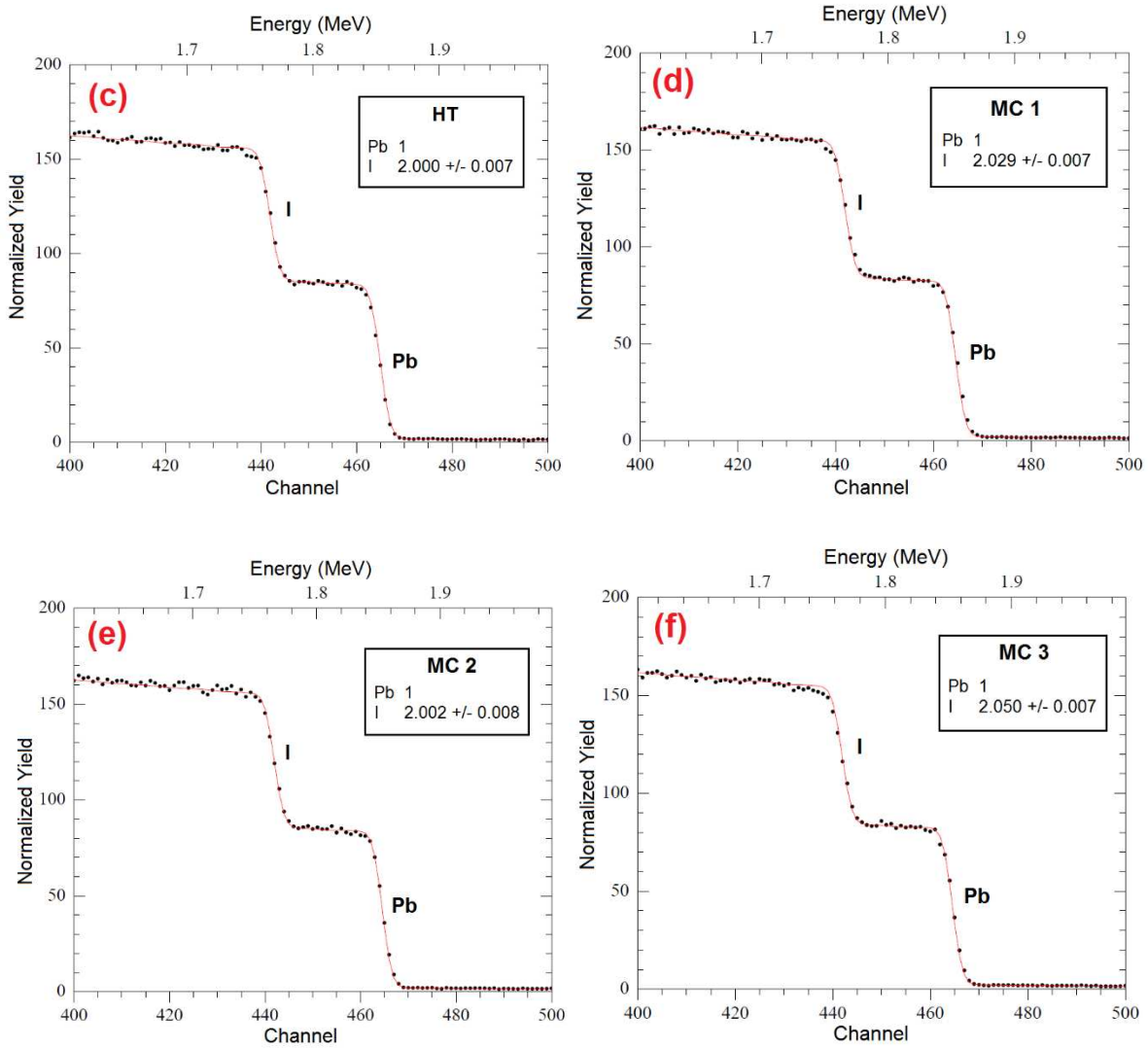

Figure S3. RBS spectra of commercial and synthesised lead iodide samples, with stoichiometric ratios between the lead and iodide. (a) SA, (b) TCI, (c) HT, (d) MC 1, (e) MC 2 and (f) MC 3 PbI_2 powders. All spectra correspond to a single point of analysis using RBS.

Table S3. Stoichiometric ratios between lead and iodide of different lead iodide samples, as determined by RBS characterisation. The samples include commercial (SA and TCI), hydrothermal (HT) and mechanochemically synthesized under different conditions (MC 1 to 3) PbI_2 powders. All values correspond to a single point of analysis as determined by RBS.

Lead iodide sample	Synthesis conditions/ sample information	Ratio of Pb:I
MC3	Mechanochemical (400 rpm 4 hours)	1:2.05 (± 0.007)
MC2	Mechanochemical (400 rpm 1 hour)	1:2.002 (± 0.008)
MC1	Mechanochemical (200 rpm 2 hours)	1:2.029 (± 0.007)
HT	Hydrothermal (in water)	1:2.0 (± 0.007)
TCI	Tokyo Chemical Industries 99.99%	1:2.009 (± 0.007)
SA	Sigma Aldrich 99.999%	1:1.9 (± 0.008)

Table S4. Percentage of the unreacted PbI_2 in $CH_3NH_3PbI_3$ micro-crystals, as a function of the system's temperature and source of PbI_2. All percentages calculated in respect to the XRD peaks that correspond to planes with Miller indices (001) for the PbI_2 and (002) / (110) for the $CH_3NH_3PbI_3$ of tetragonal crystal structure.

	Percentage (%) of unreacted PbI_2	
Temperature (ºC)	MC 2 / CH_3NH_3I equimolar	SA / CH_3NH_3I equimolar
20	14.5	52.5
50	3.1	10.9
70	4.5	11.4
90	3.9	15.7

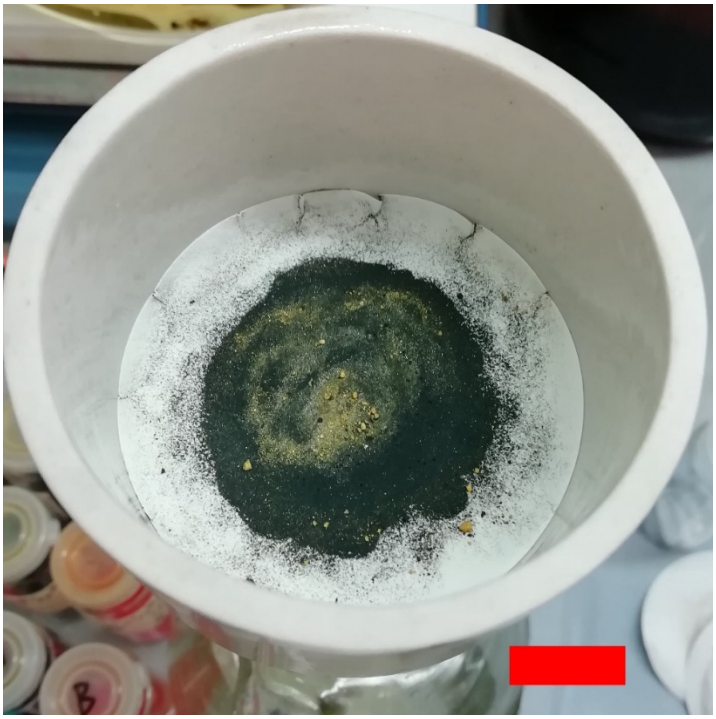

Figure S4: Unreacted PbI_2 powder (yellow in colour) in the synthesised powder of the $CH_3NH_3PbI_3$ micro-crystals synthesised using equimolar amounts of the sub-stoichiometric SA PbI_2 and CH_3NH_3I under a constant temperature of 20 ºC for 24 hours, scale bar represents 10 mm.

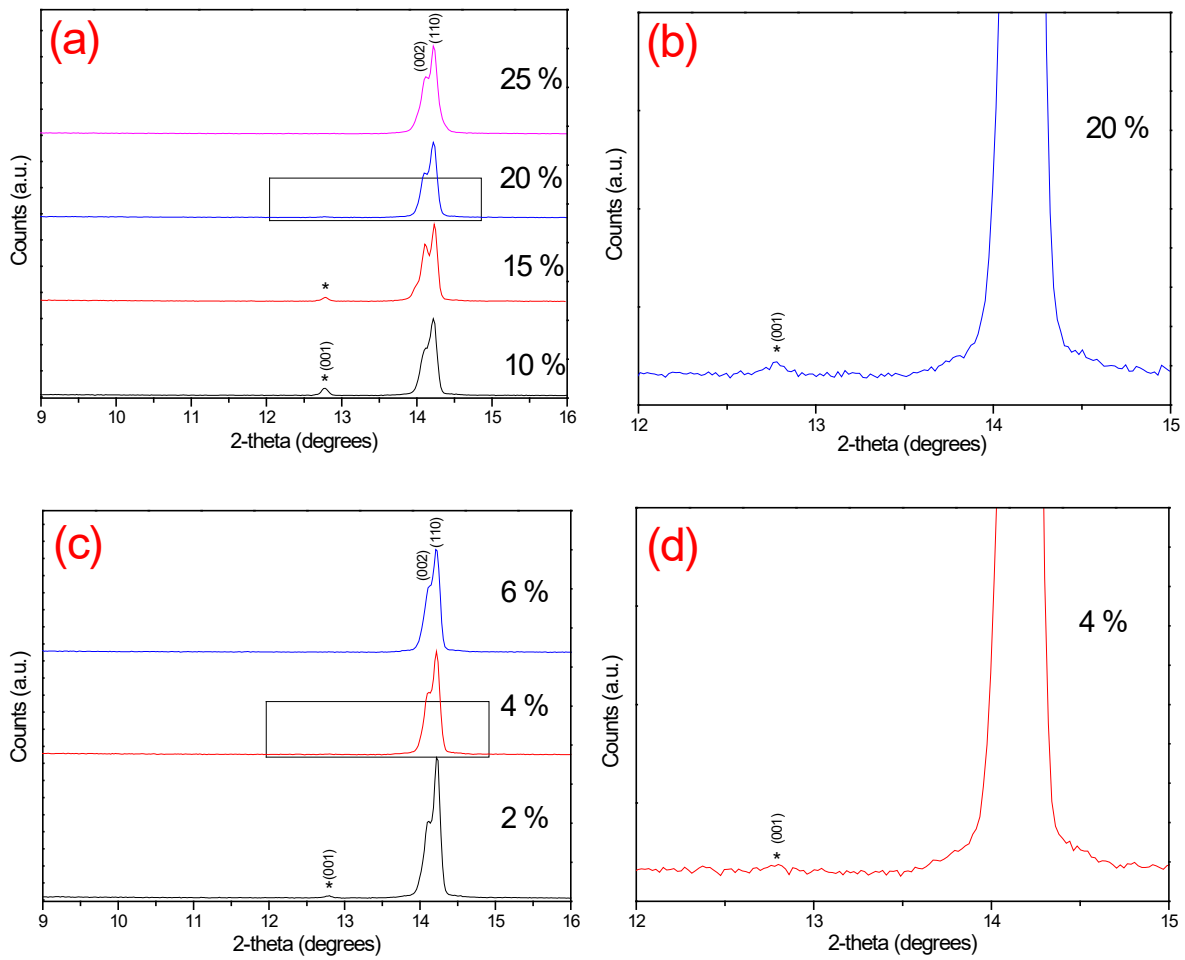

Figure S5. XRD patterns shown are from $CH_3NH_3PbI_3$ micro-crystals synthesized from (a) commercial SA PbI_2 and 10 %, 15 %, 20 % and 25 % excess CH_3NH_3I by weight, (b) commercial SA PbI_2 and 20 % excess CH_3NH_3I by weight, at higher magnification, (c) almost stoichiometric MC 2 PbI_2 and 2 %, 4 % or 6 % excess CH_3NH_3I by weight, and (d) almost stoichiometric MC 2 PbI_2 and 4 % excess CH_3NH_3I by weight, higher magnification. Asterisk marks correspond to the XRD peak of the lead iodide for crystallographic planes with Miller indices (001). The XRD peaks with Miller indices (002) and (110) correspond to the tetragonal perovskite crystal structure.

Section 3: Micro-crystal formation to correct the stoichiometry

The system of 1 - pentanol / PbI_2 / CH_3NH_3I was used to synthesise $CH_3NH_3PbI_3$ micro - crystals, by reacting sub-stoichiometric SA PbI_2 with a controllable excess of CH_3NH_3I (10 %, 15 %, 20 % and 25 % by weight of CH_3NH_3I) for 24 hours at constant temperature of 90 ºC or almost stoichiometric MC 2 PbI_2 with a controllable excess of CH_3NH_3I (2 %, 4 % or 6 % by weight of CH_3NH_3I) for 24 hours at constant temperature of 90 ºC, as well.

Figures S6a and S6b show that when 20 % more CH_3NH_3I by weight was used in reaction with the sub-stoichiometric SA PbI_2 there was almost elimination of unreacted PbI_2 as indicated from the XRD spectra. Therefore, the stoichiometry of the PbI_2 was calculated as follows:

0.5 g of sub-stoichiometric SA was mixed with a nominally equimolar amount of CH_3NH_3I plus 20 % excess by weight (0.1724 g + 0.0345 g). 0.0345 g was the mass of excess CH_3NH_3I which corresponds to 0.0069 g of $CH_3NH_3^+$, based on the summation of atomic mass units of carbon (12.0107 a.m.u.), hydrogen (1.0079 a.m.u.) and nitrogen (14.0067 a.m.u), while 0.0276 g was the mass of I^- with atomic mass unit of 126.9045 a.m.u.. Therefore, had the PbI_2 been stoichiometric the mass that would have been needed to react with the (0.1724 g + 0.0345 g = 0.2069 g) CH_3NH_3I assuming all the SA PbI_2 reacts would have been 0.5 g + 0.0276 g = 0.5276 g. i.e. (the mass of SA PbI_2 used) + (the mass of I^- that was added). To calculate the actual stoichiometry of the SA PbI_2 first the number of PbI_2 molecules is determined by taking the new corrected weight of PbI_2 divided by the molecular weight of PbI_2 (461.01 g * mol^{-1}) and multiplying by the Avogadro number (6.022 * 10^{23} molecules * mol^{-1}) which gives 6.8918 * 10^{20} PbI_2 molecules. However, in each of these molecules there are 3 atoms (1 atom of lead and 2 atoms of iodide), resulting in a total of 20.6754 * 10^{20} atoms. 66.6 % (13.7836 * 10^{20} atoms) of these are iodide atoms. The remaining 33.3% are Pb atoms (6.8918 * 10^{20} atoms). However, 0.0276 g of the iodide came from the excess CH_3NH_3I required. So, by dividing the mass of excess I^- required (0.0276 g), by the molecular weight of I^- (126.9045 g * mol^{-1}) and multiplying with the Avogadro number (6.022 * 10^{23} atoms * mol^{-1}), results in 1.3097 * 10^{20} being the number of I^- ions the PbI_2 was initially lacking. The number of iodide atoms actually present was 13.7836 * 10^{20} atoms less 1.3097 * 10^{20} = 12.4739 * 10^{20}. The final ratio between the Pb : I ratio of the sub-stoichiometric SA is 1: (12.4739 * 10^{20} / 6.8918 * 10^{20}) or 1 : 1.81. However, since we detected a weak XRD peak that corresponds to PbI_2, as shown in SI Figure SI6b. We estimate that the amount of excess CH_3NH_3I used, should be ~ 21 – 22 % more CH_3NH_3I by weight, leading to complete elimination of unreacted PbI_2, during the synthesis of $CH_3NH_3PbI_3$ micro-crystals when sub-stoichiometric SA material used. If 22 % excess by weight of CH_3NH_3I, was used. The resulting ratio between the Pb : I atoms of the sub-stoichiometric SA is 1 : 1.79. The same methodology applied, when 4 % more CH_3NH_3I by weight was used in reaction

with the almost stoichiometric MC 2, during the synthesis of $CH_3NH_3PbI_3$ micro-crystals. Resulting in a ratio between the Pb : I atoms of the almost stoichiometric MC 2 being 1 : 1.96.

During the synthesis of $CH_3NH_3PbI_3$ micro – crystals, by reacting PbI_2 with a controllable excess of CH_3NH_3I, any excess of $CH_3NH_3^+$ and I^- ions end up dissolved in the 1-pentanol. At equilibrium conditions any deficiency in the iodine ions present in the PbI_2 is corrected by the iodine ions extracted from the excess of CH_3NH_3I added. Similarly, any $CH_3NH_3^+$ ions originating from the excess of CH_3NH_3I used will dissolve in the 1 – pentanol, affecting the chemical potential of the system.[7] Additionally, any further excess of CH_3NH_3I added will dissolve in the 1 – pentanol. A further step that prevents the recrystallization of excess CH_3NH_3I from the 1 – pentanol during the vacuum filtration process is the use of a large volume of 1-pentanol, which reduces the probability of the ions ($CH_3NH_3^+$ and I^-) interacting. After completion of the chemical reaction the 1 - pentanol / PbI_2 / CH_3NH_3I solution must be kept warm and filtered as fast as possible. Unreacted $CH_3NH_3^+$ and I^- ions remain dissolved in the warm 1-pentanol and are therefore removed upon filtration.

Section 4: How iodide deficiency affects perovskite formation

To understand the presence and formation of unreacted PbI_2 in the $CH_3NH_3PbI_3$ when sub-stoichiometric PbI_2 is used, the following theory was developed based on the general chemical formula of perovskite, ABX_3, which requires the presence of 3 halogen atoms. Specifically, in $CH_3NH_3PbI_3$ formation two iodide atoms originate from the PbI_2 while one iodide atom originates from CH_3NH_3I. That requires both reactants (PbI_2 and CH_3NH_3I) being stoichiometrically perfect. However, when sub-stoichiometric PbI_2 is used, its correct chemical formula must be written as PbI_x with $1< x <2$. The percentage of unreacted PbI_2 within the $CH_3NH_3PbI_3$ when sub-stoichiometric PbI_x is used could be calculated from the mathematical equation 1:

$$\left(\left(1 - (x \div 2)\right) * 2\right) * 100\ \% \qquad \text{(equation 1)}$$

where x is the number of iodide ions in the initially sub-stoichiometric PbI_x used. $\left(1 - (x \div 2)\right)$ is the fraction of iodide missing from the initially sub-stoichiometric PbI_x used and 2 is the number of iodide ions that are needed for the formation of unreacted

PbI_2. To examine this approach a few examples are provided in Table S5. Based on the previous analysis, if more iodide is missing from the initially sub-stoichiometric PbI_x used in the synthesis of $CH_3NH_3PbI_3$ this raises the amount of unreacted PbI_2. Also, a similar trend is calculated for the remaining $CH_3NH_3^+$ ions that do not participate in the chemical reaction.

Table S5. Examples of chemical reactions between sub-stoichiometric PbI_x and CH_3NH_3I towards the formation of $CH_3NH_3PbI_3$ and resulting in unreacted PbI_2 and $CH_3NH_3^+$ ions.

Chemical reaction	**$PbI_{1.65}$ + CH_3NH_3I**	**$PbI_{1.92}$ + CH_3NH_3I**
Total number of ions	1 Pb^+ 1 $CH_3NH_3^+$ 2.65 I^-	1 Pb^+ 1 $CH_3NH_3^+$ 2.92 I^-
Total number of ions forming the $CH_3NH_3PbI_3$	0.65 Pb^+ 0.65 $CH_3NH_3^+$ 1.95 I^- or (0.65 $CH_3NH_3PbI_3$)	0.92 Pb^+ 0.92 $CH_3NH_3^+$ 2.76 I^- or (0.92 $CH_3NH_3PbI_3$)
Total number of ions for unreacted PbI_2	0.35 Pb^+ 0.7 I^- or (0.35 PbI_2)	0.08 Pb^+ 0.16 I^- or (0.08 PbI_2)
Total number of $CH_3NH_3^+$ ions	0.35 $CH_3NH_3^+$	0.08 $CH_3NH_3^+$

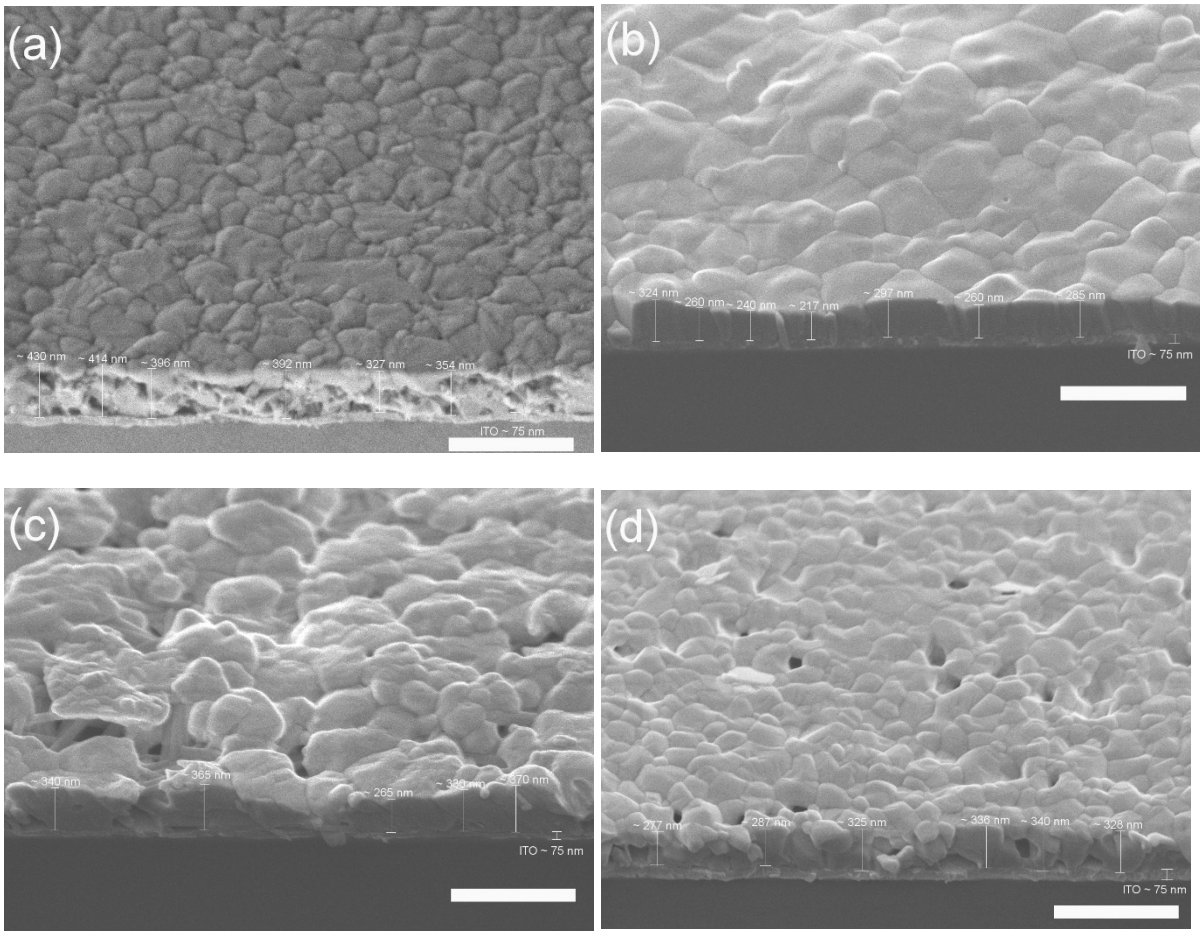

Figure S6. Cross-section Scanning electron microscopy (SEM) images of tilted at 45 deg. perovskite thin films fabricated using, (a) equimolar amounts of SA / CH_3NH_3I, (b) equimolar amounts of MC 2 / CH_3NH_3I, (c) $CH_3NH_3PbI_3$ micro-crystals using SA and (d) $CH_3NH_3PbI_3$ micro-crystals using MC 2. Scale bars represent 1 μm. The numerical length values on the SEM images are the thicknesses as observed with the sample tilted by 45°. The actual film thicknesses can be determined by dividing these as observed length values by cos (45°).

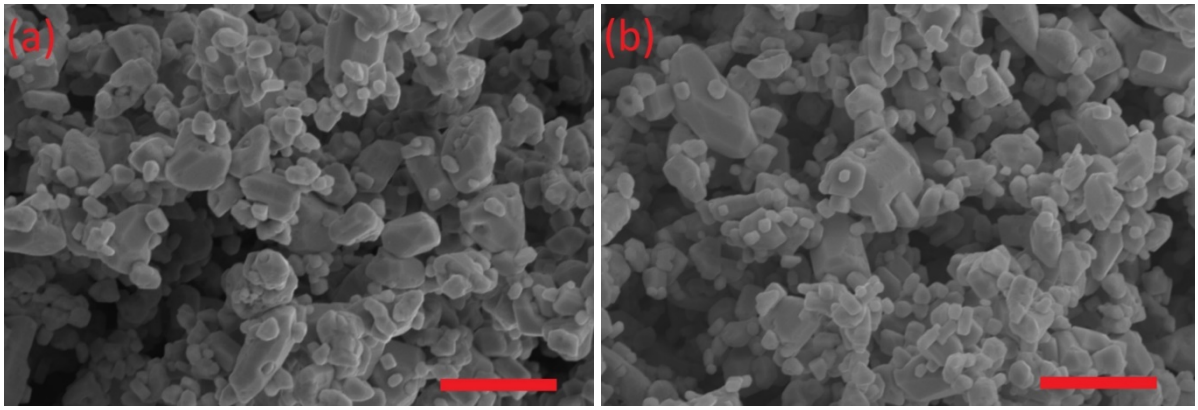

Figure S7. Scanning electron microscopy (SEM) images of $CH_3NH_3PbI_3$ micro-crystals synthesised at temperature 90 °C, using the two varieties of the PbI_2, (a) mechanochemical MC 2 and (b) SA, in reaction with 30 % more by weight of CH_3NH_3I, scale bars represent 10μm.

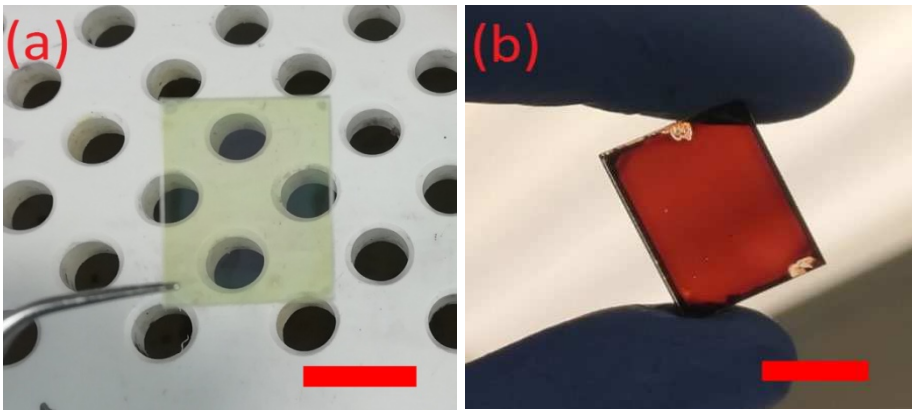

Figure S8. Images of glass / ITO / SnO_2 / perovskite after (a) extracting the DMSO under vacuum for 120 s before annealing and (b) annealing at 100 °C for 30 s, scale bars represent 10 mm.

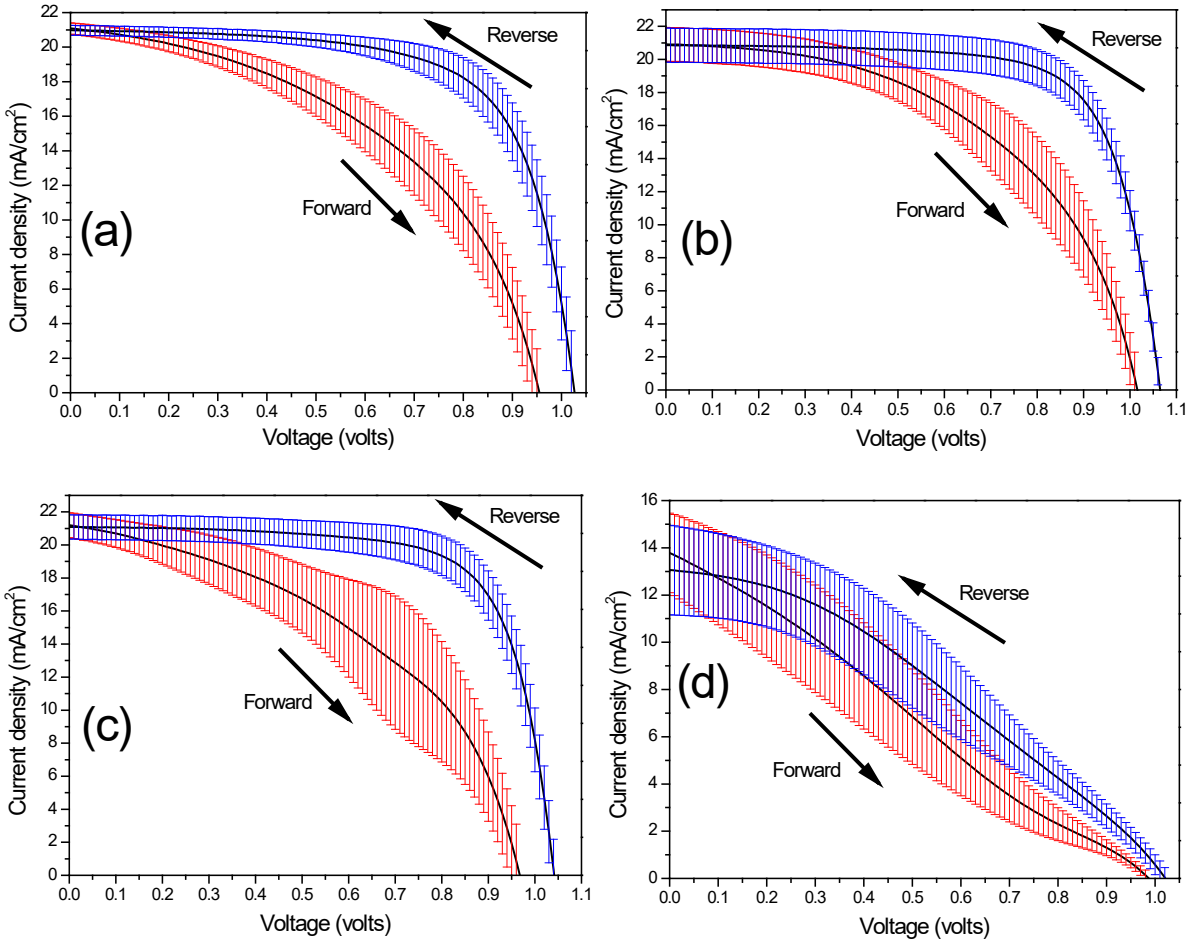

Figure S9. Characteristic current density – voltage curves in forward (0 → V_{OC}) and reverse (V_{OC} → 0) scans of PSC devices with structure glass / ITO / SnO_2 / $CH_3NH_3PbI_3$ / Spiro - OMeTAD / Au, as function of the photoactive layer fabricated using either $CH_3NH_3PbI_3$ micro-crystals or equimolar amounts of different PbI_2 with CH_3NH_3I. (a) $CH_3NH_3PbI_3$ micro-crystals made using almost stoichiometric MC2 PbI_2, (b) $CH_3NH_3PbI_3$ micro-crystals made using sub-stoichiometric SA PbI_2, (c) equimolar amounts of almost stoichiometric MC2 PbI_2 / CH_3NH_3I and (d) equimolar amounts of sub-stoichiometric SA PbI_2 / CH_3NH_3I. Black curves correspond to the average of all recorded current density – voltage curves and coloured stripes to their deviation from the average black curve. Red and blue coloured stripes, indicate current density – voltage data collected in forward (0 → V_{OC}) and reverse (V_{OC} → 0) scans, respectively.

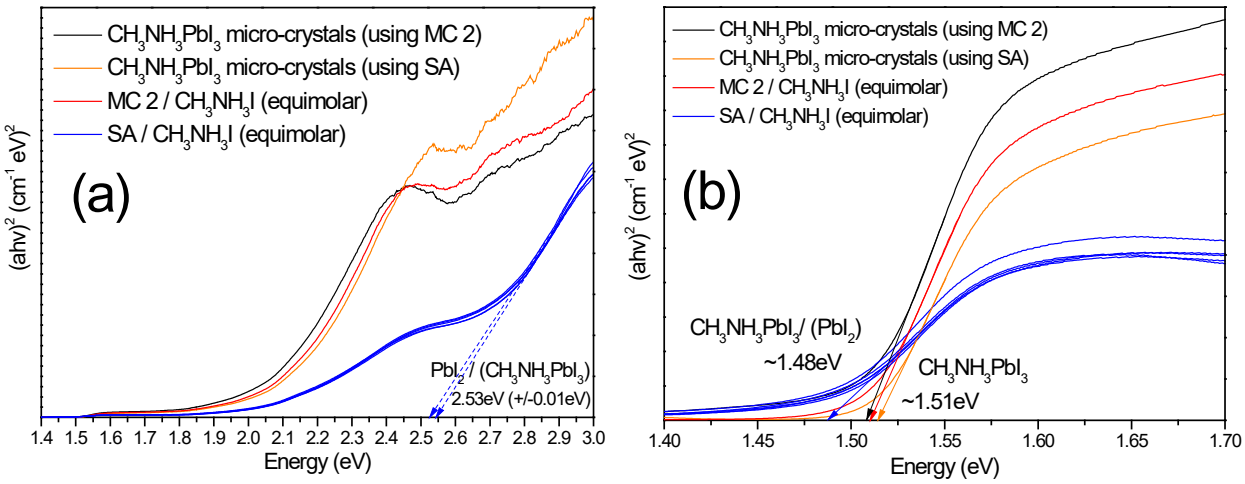

Figure S10. (a) and (b) Tauc plots of perovskite thin films synthesised using, $CH_3NH_3PbI_3$ micro-crystals (using MC 2) (black curves), $CH_3NH_3PbI_3$ micro-crystals (using SA) (orange curves), equimolar amounts of MC 2 / CH_3NH_3I (red curves), equimolar amounts of SA / CH_3NH_3I (blue curves) (from five different measured points). PbI_2 / ($CH_3NH_3PbI_3$) optical band gap (~2.53 ±0.01 eV) is indicated with blue dashed arrows. $CH_3NH_3PbI_3$ optical band gaps (~1.51 eV) are indicated with black / red / orange arrows. Whereas, $CH_3NH_3PbI_3$ / (PbI_2) optical band gap (~1.48 eV) is indicated with blue arrow.

Table S6. Fitting parameters and estimated lifetime of different perovskite samples deposited on SnO_2/ITO/glass substrates.

Sample	**λ (nm)**	**A_1**	**t_1 (ns)**	**A_2**	**t_2 (ns)**	**A_3**	**t_3 (ns)**	**<t> (ns)**
Equimolar SA / CH_3NH_3I	770	0.40	7.66	0.60	21.5	-	-	15.9
Equimolar MC 2 / CH_3NH_3I	770	0.18	0.55	0.43	6.17	0.39	15.4	8.7
Micro-crystals using SA	770	0.39	7.25	0.61	22.2	-	-	16.4
Micro-crystals using MC 2	780	0.35	6.31	0.65	17.9	-	-	13.8

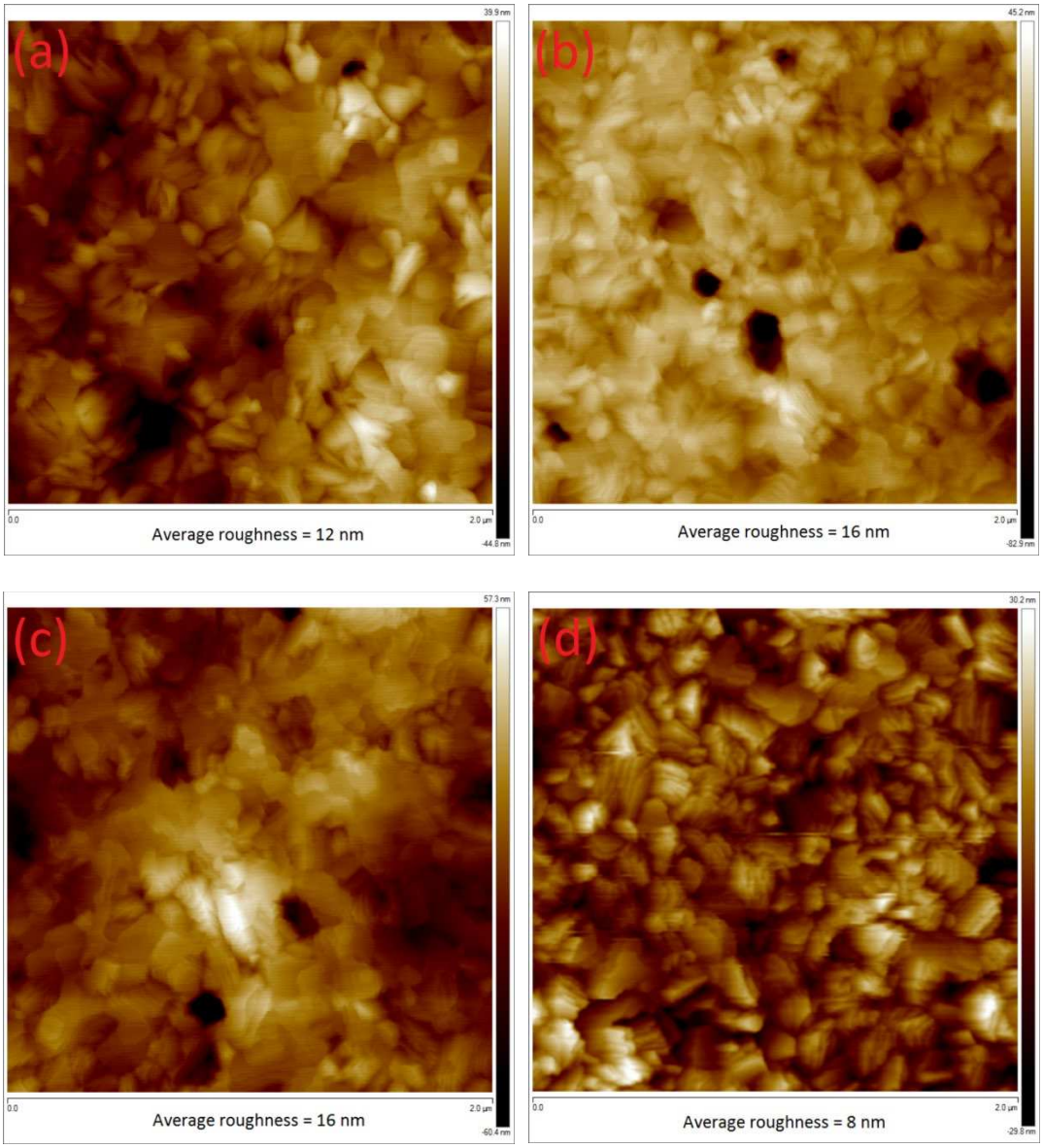

Figure S11. AFM images of perovskite thin films fabricated using, (a) $CH_3NH_3PbI_3$ micro-crystals using MC 2, (b) $CH_3NH_3PbI_3$ micro-crystals using SA, (c) equimolar amounts of MC 2 / CH_3NH_3I, (d) equimolar amounts of SA / CH_3NH_3I. The average values of roughness, are listed below each image.

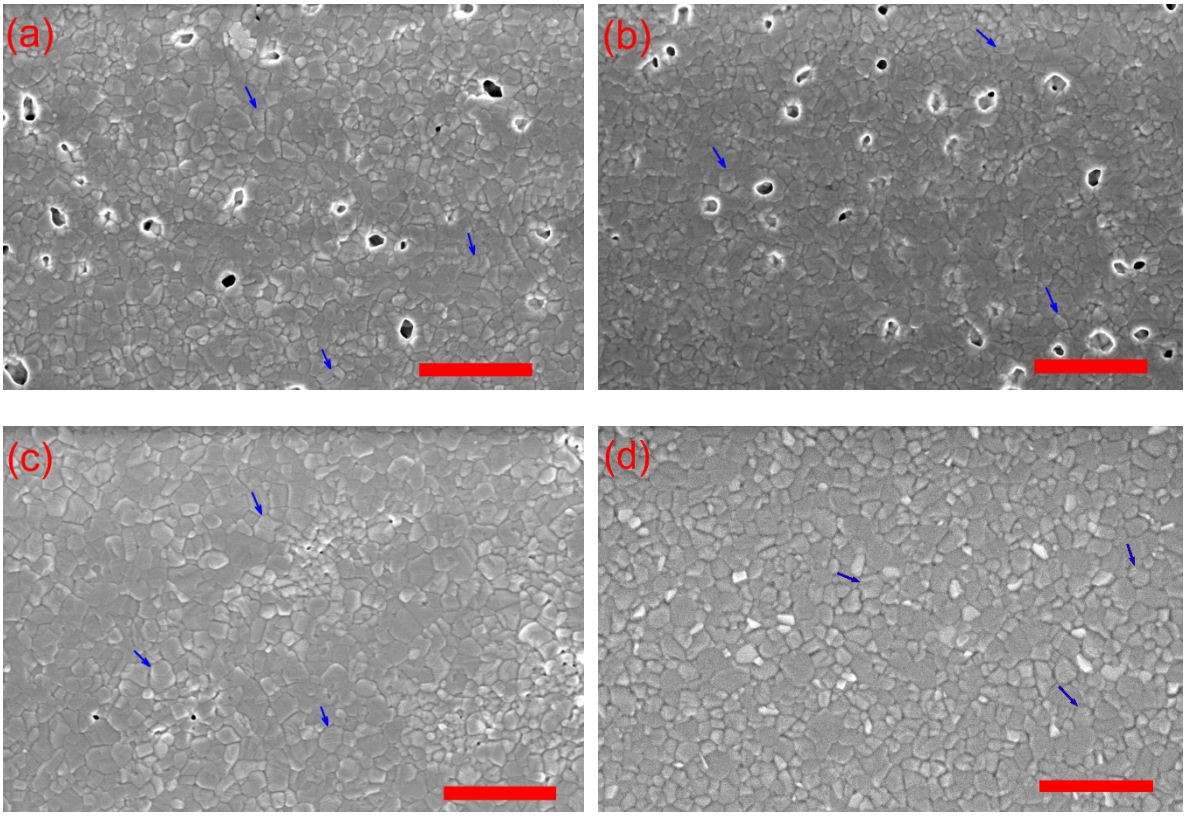

Figure S12. Low voltage scanning electron microscopy (LV-SEM) images of perovskite thin films fabricated using, (a) $CH_3NH_3PbI_3$ micro-crystals using MC 2, (b) $CH_3NH_3PbI_3$ micro-crystals using SA, (c) equimolar amounts of MC 2 / CH_3NH_3I, (d) equimolar amounts of SA / CH_3NH_3I. Layered perovskite grains, are indicated with blue arrows in all images. Scale bars represent 1 μm.

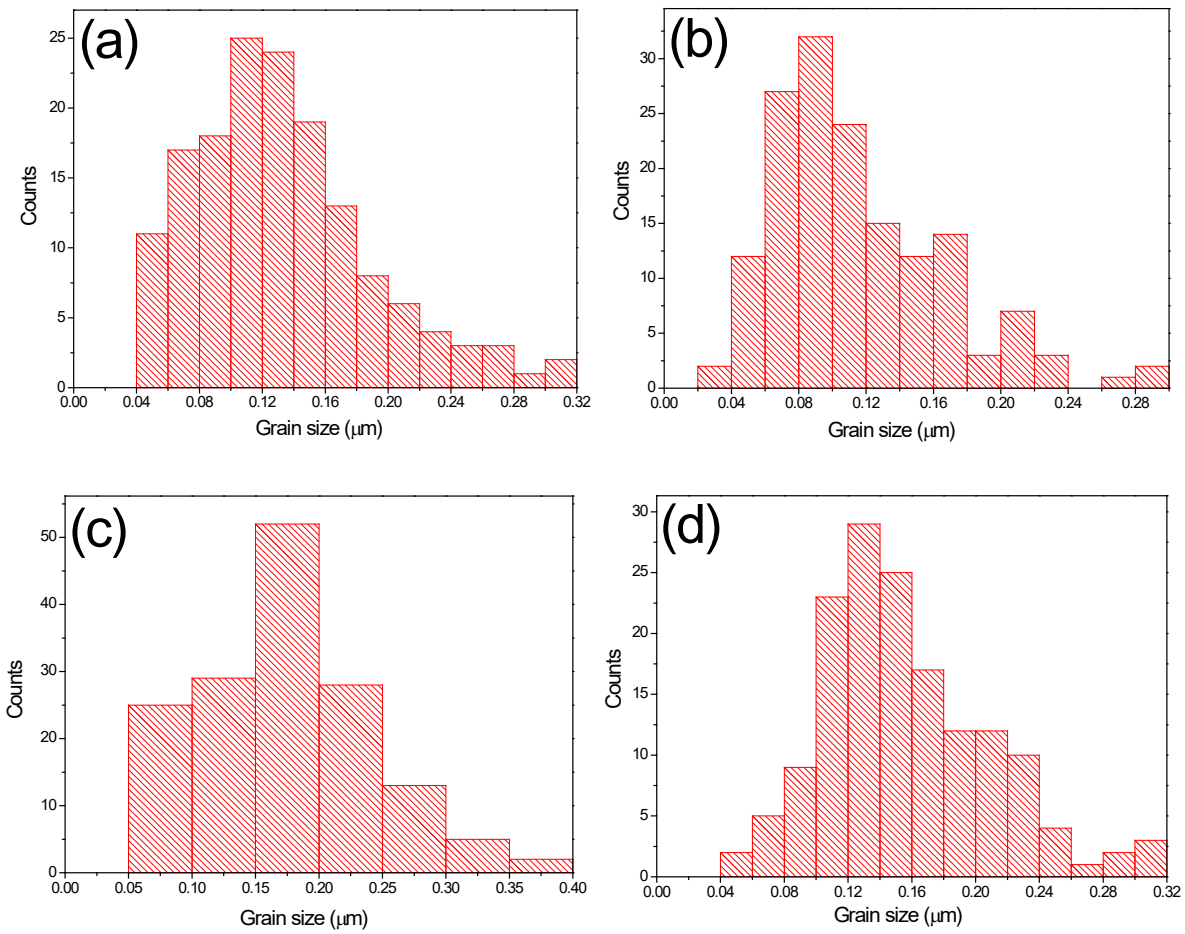

Figure S13. Grain size distribution of $CH_3NH_3PbI_3$ thin films (based on TLD - SEM images) fabricated using, (a) $CH_3NH_3PbI_3$ micro-crystals made using almost stoichiometric MC2 PbI_2, (b) $CH_3NH_3PbI_3$ micro-crystals made using sub-stoichiometric SA PbI_2, (c) equimolar amounts of almost stoichiometric MC2 PbI_2 / CH_3NH_3I and (d) equimolar amounts of sub-stoichiometric SA PbI_2 / CH_3NH_3I.

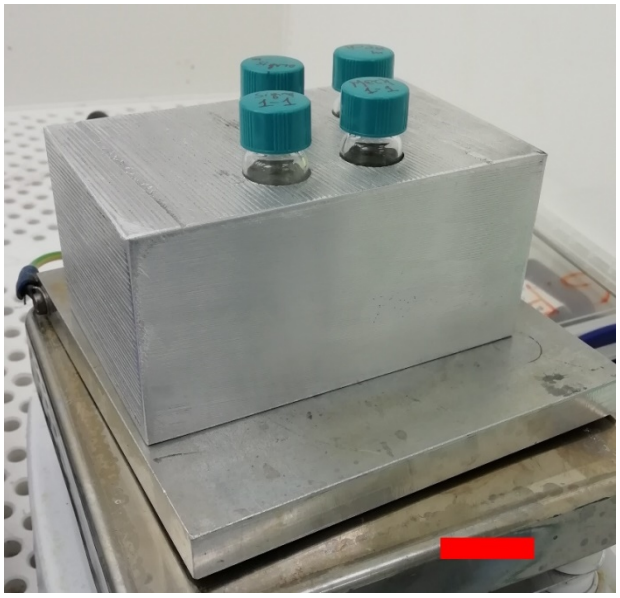

Figure S14. Image of the aluminium block used to warm the perovskite solutions whilst under constant stirring (~ 300 rpm) at a temperature of 65 ~ 70 °C. Scale bar represents 20 mm.

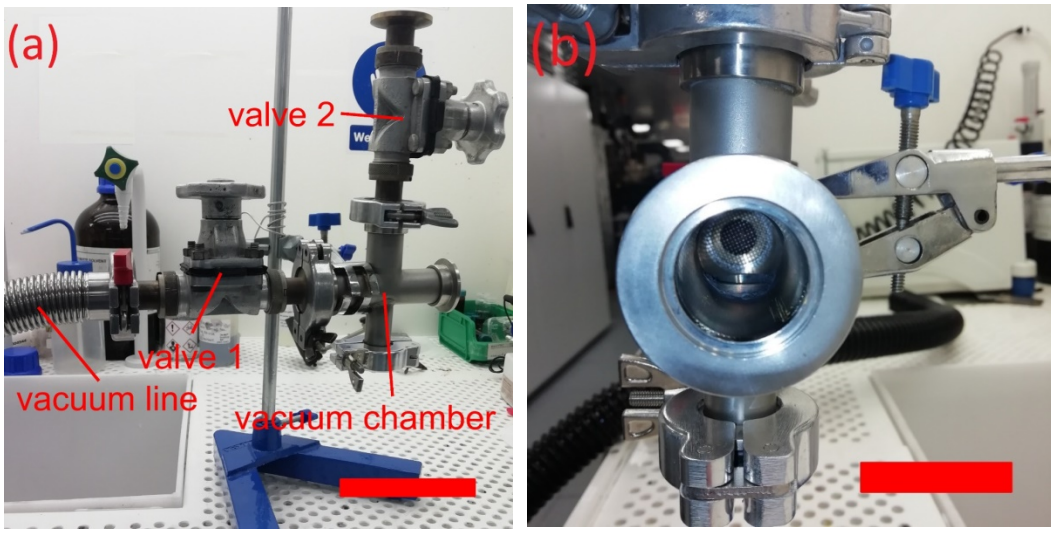

Figure S15. The vacuum chamber consisting of a vacuum line connected to a rotary vane dual stage mechanical vacuum pump (Edwards), valve 1 regulates the pressure and valve 2 resets the pressure to one bar in the vacuum chamber, respectively (a), scale bar represents 10 cm. Inside view of the vacuum chamber (b), scale bar represents 2 cm.

References

(1) Frank F.C.. Crystal dislocations, elementary concepts and definitions. Dublin Phi*losophical Mag. J. Sci.,* **1951**, **42**, 809–819.

(2) Pandey D., Krishna P.. THE ORIGIN OF POLYTYPE STRUCTURES. *Prog. Cryst. Growth and Charact.,* **1983**, **7**, 213–258.

(3) Mitchell R.S.. Structural polytypism of lead iodide and its relationship to screw dislocations. *Zeitschrift für Krist.,* **1959**, 384, 372–384.

(4) Sebastian M.T., Krishna P.. Single crystal diffraction studies of stacking faults in close-packed structures. *Prog. Cryst. Growth and Charact.,* **1987**, 14, 103–183.

(5) Ramsdell L.. Studies on silicon carbide. *Am. Mineral.,* **1947**, 32, 64–82.

(6) Mcgettrick J.D., Hooper K., Pockett A., Baker J., Troughton J., Carnie M., Watson T.. Sources of Pb (0) artefacts during XPS analysis of lead halide perovskites. *Mater. Lett.,* **2019**, 251, 98–101.

(7) Yin W.J.,Shi T.,Yan Y..Unusual defect physics in $CH_3NH_3PbI_3$ perovskite solar cell absorber. *App. Physics Lett.,* **2014**, 104(6),063903.